European Journal of Pharmaceutical Sciences 138 (2019) 105038

Contents lists available at ScienceDirect

European Journal of Pharmaceutical Sciences

journal homepage: www.elsevier.com/locate/ejps

Antioxidant properties of probucol released from mesoporous silica

Michael Lau[a], Kalpeshkumar Giri[a,b], Alfonso E. Garcia-Bennett[a,b,*]

[a] Department of Molecular Sciences, Macquarie University, Sydney, NSW 2109, Australia
[b] Australian Research Council Centre for Nanoscale Biophotonics, Macquarie University, Sydney, NSW 2109, Australia.

ARTICLE INFO

Keywords:
Drug delivery
Pharmaceutical excipients
Antioxidant properties
Probucol
Mesoporous silica

ABSTRACT

Antioxidants play a vital role in scavenging reactive oxygen species (ROS) produced by the reduction of molecular oxygen from various cellular mechanisms. Under oxidative stress, an increase in the levels of ROS overwhelms the antioxidant response, causing oxidative damage to biological molecules, and leading to the development of various diseases. Drug compounds with potent antioxidant properties are typically poorly water soluble and highly hydrophobic. An extreme case is Probucol (PB), a potent antioxidant with reported water solubility of 5 ng/ml, and oral bioavailiability of < 10%. In this study, PB was loaded in mesoporous silica at various drug loadings to understand the changes to the physical properties of the loaded drug, and it's *in vitro* drug release. Further *in vitro* studies were conducted in endothelial and microglia cell models to compare the free radical scavening efficiency of ascorbic acid, PB, and PB release from mesoporous silica particles.

Out of the three different mesostructured particles studied, the maximum loading of PB was achieved for large pore mesoporous particles (SBA-15) at 50 wt% drug loading, before complete pore filling was observed. For all materials, loadings above complete pore filling resulted in the recrystallization of PB on the external surface. *In vitro* drug release measurements showed a rapid dissolution rate at low drug loadings compared to a bimodal release profile of amorphous and crystalline drug at higher drug loadings. PB loaded in mesoporous particle was shown to enhance the antioxidant response to extracellular ROS in the endothelial cell line model, and to intracellular ROS in the microglia cell model.

Our results indicate that the antioxidant properties of PB can be significantly improved by using mesoporous silica as a delivery vehicle.

1. Introduction

Reactive oxygen species (ROS) are highly unstable oxygen carrying free radicals that cause oxidative damage to biological molecules including DNA, proteins, and lipids (Di Meo et al., 2016). The reduction of molecular oxygen by intracellular mechanisms results in the production of endogenous ROS (Di Meo et al., 2016). Examples include peroxyl, superoxide anion, and hydroxyl radicals (Pourova et al., 2010). Exogenous sources of ROS include exposure to xenobiotics, radiation, and toxic chemicals (Pourova et al., 2010). Furthermore, ROS are involved in important cellular processing and signaling pathways which are vital for normal cell functioning (Pourova et al., 2010). A steady state concentration of ROS is maintained by antioxidant defense mechanisms that act as free radical scavengers in protecting biological molecules against oxidative damage.

Antioxidant defense mechanisms can be classified into two categories: antioxidant enzymes, and chain-breaking antioxidants. Antioxidant enzymes are produced endogenously and include the superoxide dismutase (SOD), catalase, and glutathione peroxidases (Birben et al., 2012). These enzymes catalyze the conversion of ROS into a more stable, unreactive molecule. Chain-breaking antioxidants are free radical scavengers that convert ROS into a more stable unreactive molecule (Padayatty et al., 2003). These antioxidants can be further classified as water or fat soluble. Ascorbic acid is a highly potent water soluble antioxidant that can scavenge a range of intracellular and extracellular ROS, including superoxide, hydroxyl and hydrogen peroxide (Padayatty et al., 2003). Vitamin E is the most important fat soluble antioxidant that is found in cellular membranes, protecting it from oxidative damage by ROS (Padayatty et al., 2003).

Under oxidative stress, increased concentrations of ROS overwhelms the antioxidant defense mechanisms, causing oxidative damage to cells and the development in pathological conditions such as diabetes, cancer, and cardiovascular diseases (Birben et al., 2012; Day, 2004). In diabetes, increasing evidence implicate oxidative stress in impaired glucose metabolism, and the development of complications including hypertension, atherosclerosis, and nephropathy (Baynes, 1991). Despite

* Corresponding author at: Department of Molecular Sciences, Macquarie University, Sydney, NSW 2109, Australia.
E-mail address: alf.garcia@mq.edu.au (A.E. Garcia-Bennett).

https://doi.org/10.1016/j.ejps.2019.105038
Received 23 April 2019; Received in revised form 15 July 2019; Accepted 5 August 2019
Available online 06 August 2019
0928-0987/

the evidence on the role of oxidative stress in these diseases, the effectiveness of treatment with antioxidant supplementation such as ascorbic acid or vitamin E has been inconclusive (Balbi et al., 2018; Kizhakekuttu and Widlansky, 2010).

Instead, drug compounds with antioxidant properties are being investigated for the treatment of diseases caused by oxidative stress. The statins rosuvastatin (Holvoet, 2008), atorvastatin (Wassmann et al., 2002), and simvastatin (Chartoumpekis et al., 2010) have antioxidant properties that inhibit LDL (low density lipoprotein) oxidation independent of the drug's effect in lowering LDL levels. Oral hypoglycemic medications including gliclazide (O'Brien et al., 2000), metformin and pioglitazone were shown to have antioxidant activities, inhibit LDL oxidation, and increase antioxidant levels from *in vivo* studies in diabetic patients (O'Brien et al., 2000; Singh et al., 2016). In patients with hypertension, production of ROS and markers of lipid oxidation are increased, and levels of the antioxidant SOD and glutathione are decreased (Rodrigo et al., 2007; Redón et al., 2003). Antihypertensive medications metoprolol and carvedilol was shown in an *in vivo* human study to reduce thiobarbituric acid reactive substances considered a marker of oxidative stress (Kukin et al., 1999), amlodipine was shown to increase levels of SOD and reduce oxidative stress in patients with hypertension (Mahajan et al., 2007), and enalapril was shown to reduce oxidative stress markers, and increase antioxidant enzyme levels in diabetic rats (de Cavanagh et al., 2001).

Probucol is an antioxidant containing two butylated hydroxytoluene moieties (Kuzuya and Kuzuya, 1993). It is a potent free radical scavenger, and is used to inhibit lipid oxidation in the treatment of atherosclerosis, xanthoma, and cardiovascular diseases (Barnhart et al., 1989; Kuzuya and Kuzuya, 1993). Due to its potent antioxidant properties, there has been renewed interest in expanding the clinical use of PB in diseases such as type II diabetes, restenosis after angioplasty, and diabetic nephropathy (Yamashita et al., 2015). However, PB's extreme physicochemical properties make it highly challenging in achieving favorable pharmacokinetics from oral administration. It is a non-ionizable, highly lipophilic drug compound with a partition coefficient of 8.9, water solubility of 2–5 ng/ml, and reported oral bioavailability of < 10% (Nielsen et al., 2008) ranking it among the most poorly soluble, and hydrophobic drug compound with known antioxidant activity (Fig. 1).

Various formulation strategies have been used to improve the dissolution rate of PB including dry/wet milling, spray drying, and nanoemulsions (Thybo et al., 2008; Li et al., 2017; Zhang et al., 2014). The enhancement in % PB release of 30% at 2 h was achieved from a co-milled formulation containing surfactant and polymer, compared to the release of 0.68% at 2 h in a commercial PB formulation (Li et al., 2017). A spray dried formulation of PB with polymer PVP-K30 achieved a 60% of drug release after 1 h (Thybo et al., 2008). Wet milling of PB with dispersing agents gelucire, vitamin E, and pluronic F-108 was investigated by Tanaka et al. (2012). Results from *in vitro* dissolution experiments indicated the highest apparent solubility and % PB release was achieved by wet milling with vitamin E (Tanaka et al., 2012). However, concerns regarding the potential toxicity of the surfactants and polymers used in these formulations, low drug loading, and incomplete drug release highlight the extreme challenge in formulating PB for oral administration.

Mesoporous silica are ordered porous materials characterized by pore sizes between 2 and 50 nm, large surface area (up to 1000 m^2/g), and adjustable pore volume (up to 1 cm^2/g) (Wu et al., 2013). The porous properties and high surface area of mesoporous silica make it an attractive drug carrier for the delivery of high drug payloads (up to ~30%w/w) (Xu et al., 2013). Drug loaded in mesoporous silica are stabilized within the nano-confines of the mesopores in the amorphous state, due to the restriction in molecular mobility that limit the recrystallization of the loaded drug (Rengarajan et al., 2008; Prasad and Lele, 1994). The release of the amorphous drug from the mesopores has higher dissolution rate compared to its crystalline state, as demonstrated in a range of poorly soluble drug compounds (Jangra et al., 2016; Xu et al., 2013; Maleki et al., 2017). For example, a faster atorvastatin dissolution rate was achieved from the drug loaded in 2-dimensional (2d) ordered mesoporous silica SBA-15 (68% over 45 min) compared to the crystalline drug (40% over 45 min) (Maleki and Hamidi, 2016), and (Hu et al., 2012) demonstrated an enhancement in carvedilol dissolution rate of 60% over 45 min was achieved from drug loaded in 3d ordered mesoporous silica SBA-16, compared to 20% in crystalline drug. Both atorvastatin and carvedilol have very low solubility in the same range as PB, however the latter has a considerably higher Clog P (Fig. 1) making it harder to formulate in a soluble bioavailable form.

In this work, our aim is to demonstrate the enhancement in dissolution rate, and antioxidant properties of PB can be achieved by

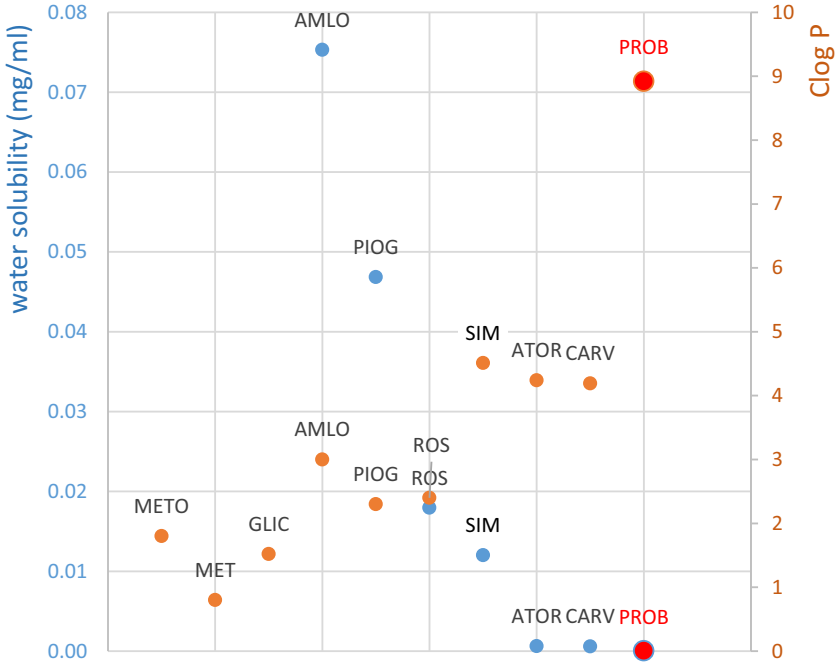

Fig. 1. Solubility in water (blue) and Clog P (orange) of poorly soluble drug compounds. Probucol (PB) has the highest calculated partition coefficient of 8.9 (Clog P) and lowest solubility in water of 2–5 ng/ml compared to the other poorly soluble drug compounds: metoprolol (METO), metformin (MET), gliclazide (GLIC), amlodipine (AMLO), pioglitazone (PIOG), rosuvastatin (ROS), simvastatin (SIM), atorvastatin (ATOR), carvedilol (CARV). (For interpretation of the references to colour in this figure legend, the reader is referred to the web version of this article.)

loading the drug in mesoporous silica. Changes in the physical properties of drug loaded samples in terms of crystallinity, surface textural properties of mesoporous silica, and drug dissolution are investigated at different drug loading amounts wt% and capsule dose. Additionally, two *in vitro* cellular models are used to investigate the antioxidant response of PB and ascorbic acid to extracellular ROS in the endothelial cell line, and to intracellular ROS in the microglia cell line.

2. Materials and methods

2.1. Chemicals and reagents

Tetraethylorthosilicate (TEOS), cetyltrimethylammonium bromide (CTAB), (3-aminopropyl)triethoxysilane (APTES), aqueous ammonia (32 wt%), pluronic p123 (p123), hydrochloric acid, ethanol, propylene bottles, hydrogen peroxide (H_2O_2), lipopolysaccharides (LPS), dimethyl sulfoxide (DMSO), probucol, ascorbic acid, Dulbecco's Modified Eagle Media (DMEM) were purchased from Sigma Aldrich (Sydney, Australia). N-lauroyl-L-alanine (C_{12}Ala) was purchased from BOC sciences (New York, USA). Fetal bovine serum (FBS), penicillin-streptomycin (10,000 U/ml), TrypLE express enzyme (TrypLE), were purchased from Thermo Fisher scientific (Victoria, Australia). Muse™ count and viability assay kit, and Muse® oxidative stress kit were purchased from Merck Millipore (Victoria, Australia). All chemicals were of reagent grade and used without further purification. Milli-Q® water was used throughout the experiments.

2.2. Synthesis of mesoporous particles

2.2.1. Synthesis of AMS-6

The synthesis of AMS-6 follows the protocol reported previously (Atluri et al., 2008). Briefly, C_{12}Ala was used as the surfactant, APTES as the co-structure directing agent (CSDA), and TEOS the silica source. A homogenous solution of C_{12}Ala (0.10 g) in Milli-Q® water (20 g) was kept at 80 °C for 24 h under static conditions. The surfactant solution was stirred for 10 min before the addition of APTES (0.10 g). After stirring for 3 min, TEOS (0.51 g) was added and the solution was stirred for 10 min at 80 °C in a closed bottle. The synthesis gel was heated at 80 °C under static conditions for 24 h. The silica product was filtered and dried at room temperature, followed by calcination at 550 °C for 3 h to remove the surfactant template.

2.2.2. Synthesis of MCM-41

The synthesis of MCM-41 followed the protocol reported previously (Grün et al., 1999). Briefly, CTAB (2.5 g) was added to Milli-Q® water (50 g), 13.2 g aqueous ammonia (32 wt%) and 60.0 g of absolute ethanol in a propylene bottle. The solution was stirred at room temperature for a period of 1 h. Subsequently, 4.7 g of TEOS was added, and the mixture was stirred for a further of 2 h. The closed propylene bottle was placed inside an oven set to 100 °C for a period of 24 h. The sample was filtered, washed with ethanol and left to dry at room temperature for 12 h. The sample was calcined in a furnace at 550 °C for 3 h.

2.2.3. Synthesis of SBA-15

The synthesis of SBA-15 followed the protocol reported previously (Kruk et al., 2000). 4 g of p123 was dispersed in 30 g water and stirred for 4 h. 120 g of 2 M hydrochloric acid solution was added and stirred for 2 h. 8.54 g of TEOS was added to the solution under stirring at 100 rpm for 20 min. The resulting gel was aged at 40 °C for 24 h and the bottle was placed inside the oven at 100 °C for 48 h. After synthesis, the solution was filtered, washed with distilled water and dried at room temperature, followed by calcination at 600 °C for 5 h.

2.3. Scanning electron microscopy (SEM)

Images were obtained using a JSM-7401F scanning electron microscope (JEOL Ltd., Tokyo, Japan) operating at 1–2 kV with no gold coating, using gentle beam mode at magnifications between 100 and 10,000.

2.4. Nitrogen adsorption/desorption isotherm

Nitrogen adsorption/desorption isotherm were measured at liquid nitrogen temperature (−196 °C) using a Micromeritics TriStar II volumetric adsorption analyzer (Micromeritics Instrument Corporation, GA, USA) for calcined and drug loaded mesoporous particle samples. Before the measurements, the samples were degassed for 3 h at 80 °C. The surface area of the samples was calculated by using the Brunauer–Emmett–Teller (BET) equation in the relative pressure (P/P_o) range of 0.05 and 0.3 (Brunauer et al., 1938). The total pore volume was calculated from the amount of gas adsorbed at P/Po = 0.95. The pore size distribution curves were derived using the density functional theory (DFT) assuming a cylindrical pore model for all samples. All calcined mesoporous materials exhibited a type IV isotherm profile, with SBA-15 displaying a type H_1 hysteresis in desorption branch. No hysteresis is observed in mesoporous AMS-6 nor MCM-41 due to the smaller pore size distribution (Ravikovitch et al., 2006).

2.5. Drug loading

PB was loaded into mesoporous silica *via* a wetness impregnation method. Briefly, the drug was dissolved in a glass beaker with ethanol. In a round bottom flask, calcined mesoporous silica was mixed with ethanol and sonicated for 10 min. The solution containing dissolved drug was added to the round bottom flask with mesoporous silica, and the mixture was mixed for 20 min. The solvent was removed by rotary evaporation at 40 °C, 150 rpm rotation at a pressure of 66 Pa. Samples were left to dry, and stored in a desiccator until further use. Samples were labelled according to the drug loading percentage. For example, AMS-6PB30% was labelled for samples containing 30% (w/w) PB loaded in mesoporous silica AMS-6.

2.6. Thermogravimetric analysis (TGA)

A Thermogravimetric Analysis instrument (TA instruments, TGA-2050, Delaware, USA) was used to determine the drug loading amount in the mesoporous particle. Analysis was conducted at a heating rate of 20 °C min^{-1} from 20 to 800 °C. The sample weights varied from 5 mg to 10 mg. The derivative weight loss calculation was performed using TA instruments software (TA instruments, Universal analysis 2000, version 3.0 G).

2.7. Differential scanning calorimetry (DSC)

Differential scanning calorimetry instrument (TA instruments, DSC-2010, Delaware, USA) was used to determine the crystallinity of the sample at a heating rate of 10 °C min^{-1} from 20 to 350 °C. The sample weights varied from 5 mg to 10 mg. Analysis was performed using TA instruments software (TA instruments, Universal analysis 2000, version 3.0 G).

2.8. Powder X-ray diffraction (XRD)

Powder XRD was performed on free drug and drug loaded samples to determine the presence of crystalline drug (Bruker D8 Discover XRD) using CuKα radiation (λ = 1.5418 Å). The diffraction patterns were recorded between 0.5 and 70° (2θ) for drug loaded samples and 1 to 8° (2θ) for unloaded calcined mesoporous samples.

2.9. Drug release

Drug release studies were conducted in simulated intestinal fluid (SIF) containing 0.25% (*w/v*) CTAB as a wetting agent. Size 1 gelatin capsules (ProSciTech, Batch: RL042, Queensland, Australia) were used to encapsulate both the pure drug and drug loaded mesoporous silica samples. Drug release was assessed under sink conditions (900 ml SIF, pH 6.8) using a UV/Vis spectrometer (Agilent, Cary 60 UV–Vis, Sydney, Australia) at λ_{Max} of 242 nm. The release was carried out in an Apparatus II dissolution bath (Agilent, 708-DS, Sydney, Australia) at a stirring rate of 50 rpm, 37 °C, and data collected approximately every 5 min for 24 h.

2.10. Cell culture

Immortalized human cerebral microvascular endothelial cells (hCMEC/D3) were kindly donated by Mr. Guoying Wang (Macquarie University, Centre for Nanoscale Biophotonics, Australia). Immortalized murine microglia cells were kindly donated by Dr. Lindsay Parker (Macquarie University, Centre for Nanoscale Biophotonics, Australia). hCMEC/D3 Cells were cultured in DMEM supplemented with 10% FBS and 1% Penicillin/Streptomycin at 37 °C with 5% CO_2, 95% fresh air, and were passaged every 5 to 7 days. Cells of passage length between 25 and 35 days were used for the *in vitro* experiments.

Microglia cells were cultured in DMEM supplemented with 10% FBS and 1% Penicillin/Streptomycin at 37 °C with 5% CO_2, 95% fresh air, and were passaged every 3 to 4 days. Cells of passage between 10 and 15 days were used for the *in vitro* experiments.

2.11. In vitro cell experiments

hCMEC/D3 Cells were seeded onto 6 well plates at a density of 2×10^6 to 4×10^6 containing 2 ml media and cultured for 5 to 7 days. On the day of the experiment, media in each of the wells was discarded. The test compound (ascorbic acid, AMS-6PB, and PB) was added together with hydrogen peroxide into each of the six well plates. Hydrogen peroxide, AMS-6 PB, and ascorbic acid was prepared in fresh media and sonicated briefly for 5 min. PB was dissolved in DMSO and was further diluted in media to a final concentration of < 0.01% (v/v). The 6 well plates were left inside the incubator for the duration of the experiment. Percentage of cells under oxidative stress, and cell viability were analyzed by the Muse® Oxidative stress kit, and Muse™ count and viability kit, respectively.

Microglia cells were seeded onto 6 well plates at a density of 2×10^6 to 3×10^6 containing 2 ml media and cultured for 1 day. 10 μg/ml LPS was added to activate microglia cells, and incubated at 37 °C with 5% CO_2, 95% fresh air for 48 h. The test compounds PB, ascorbic acid, and AMS-6 PB were incubated between 2 and 24 h. The percentage of cells under oxidative stress, and cell viability were analyzed by the Muse® Oxidative stress kit, and Muse™ count and viability kit, respectively.

2.12. Muse® oxidative stress kit

The Muse® oxidative stress kit quantitatively determines the count and percentage of cells that are under oxidative stress (%ROS +) based on intracellular detection of superoxide radicals, from cells that are not under oxidative stress (%ROS -). The Muse® oxidative stress reagent is based on dihydroethidium which is cell membrane permeable and oxidizes with intracellular free radicals to form the fluorophore ethidium bromide.

Each sample was analyzed according to the protocol provided by the manufacturer. Briefly, media was removed from the six well plates, and TrypLE was used as the dissociation agent to recover the cells. Approximately 1 ml of fresh media was added to stop the TrypLE reaction and the cell suspension was added into 15 ml falcon tubes for centrifugation at 300 *g* for 3 min. Media was removed, and PBS was added to re-suspend the cell pellet. 100 μl of cell suspension was added to 190 μl of Muse® oxidative stress reagent and incubated for 30 min. Data analysis was performed on the MUSE cell analyzer®.

2.13. Muse™ count and viability kit

The Muse™ count and viability reagent contain a DNA-binding dye that stains the nucleus of dead and dying cells. The dye does not stain the live cells, allowing for the discrimination between dead and viable (live) cells. Samples were analyzed following the protocols provided by the manufacturer. Briefly, media was removed from the six well plates, and TrypLE was used as the dissociation agent. Approximately 1 ml of fresh media was added to stop the TrypLE reaction and the cell suspension was added into 15 ml falcon tubes for centrifugation at 300 *g* for 3 min. Media was removed, and PBS was added to re-suspend the cell pellet. 10 μl of cell suspension was added to 400 μl of Muse™ count and viability reagent and incubated for 10 min. Data analysis was performed on the MUSE cell analyzer® containing the Muse™ count and viability software module that performs the calculations to determine the percentage of viable and dead cells.

3. Results and discussion

Probucol was loaded into mesoporous silica material AMS-6, with a 3d cubic mesostructure; and into MCM-41 and SBA-15, with 2d hexagonal arrangement of mesopores (Manzano et al., 2008; Atluri et al., 2008). A wetness impregnation method using ethanol as a solvent was utilized to load PB. Detailed synthetic and characterization results are included in the Electronic Supporting Information (Fig. S1). Table 1 shows a summary of structural and textural properties of PB loaded mesoporous materials. Approximately 50, 40, and 30 wt% of PB could be loaded within SBA-15, AMS-6, and MCM-41 respectively, before complete pore filling was determined from nitrogen adsorption measurements. The larger pore size of calcined SBA-15 (104.5 Å) and AMS-6 (46.7 Å) *versus* MCM-41 (31.7 Å) allowed for a larger loading amount of PB before complete pore filling was attained. To study the nature of PB adsorbed onto the external particle surface, samples were also loaded up to 60 wt%. Samples are denoted with their loading amount, *e.g.* AMS-6PB13.2% as determined from TGA analysis (Fig. S2).

The crystalline state of the drug before and after loading into mesoporous silica was investigated by XRD and DSC. There was no loss of mesoscale order as a function of drug loading < 30 wt% of PB (Figs. 2a and S3). XRD patterns at drug loadings above complete pore filling resulted in the presence of crystalline drug, likely on the surface of the silica particle (Fig. 2b). The scattering peaks from XRD do not completely correspond with those of the original crystalline polymorph (form I) but also contain another PB polymorph (form II, see also Fig. S3b), suggesting recrystallization of PB was likely to have occurred (Gerber et al., 1993). DSC scans of PB loaded mesoporous materials further confirm the presence of crystalline drug at loadings above complete pore filling, compared to the confinement within the mesopores of amorphous PB at lower drug loadings (Fig. S4). The presence of two endothermic peaks from DSC scans in high drug loaded samples (> 40 wt%) indicate a mixture of polymorphic crystals was likely present (Fig. S4). The amount of crystalline material in the samples can be estimated from the ratio in the enthalpy of melting of crystalline PB to the drug loaded mesoporous materials (Fig. 2c).

Drug loadings ≤ 40 wt% resulted in < 5% crystalline drug for the larger pore materials of SBA-15 and AMS-6; and < 10% for MCM-41. Loadings above 40 wt% resulted in a rapid increase in the %crystallinity (Fig. 2c). This was likely caused by the recrystallization of PB outside of the mesopores due to the saturation in surface area (Fig. 2d) and pore volume (Fig. S5). Furthermore, the broad endothermic peak above 50 °C, observed from the DSC thermograph at low drug loading was

Table 1
Summary of structural, porosity, and loading properties of PB within mesoporous silica particles AMS-6, MCM-41, and SBA-15; including unit cell parameters (a[a]), BET surface area (SA_{BET}), the total pore volume (T_{vol}), the pore size distribution (PSD), the drug loading amount and the drug decomposition temperature from TGA (D_T). The melting endotherm (T_m) and enthalpy (ΔH_m) are derived from DSC scans. Note that only calcined SBA-15 has 119.9 m/g of additional microporosity.

	a (Å)[a]	SA_{BET} (m^2/g)[b]	T_{vol} (cm^3/g)[c]	PSD[c] (Å)	Load (%wt)	D_T[d] (°C)	T_m (°C)	ΔH_m (J/g)
MCM-41	43.3	975.5	0.5	31.7				
AMS-6	51.8	777.3	0.7	46.7				
SBA-15	118.6	646.9	0.9	104.5				
PB						210.4	124.2	54.5
MCM-41PB	44.2	764.9	0.4	31.4	13.1	263.3		
	44.2	432.5	0.2	31.0	18.5	252.8	112.8	0.05
	44.2	273.7	0.1	30.4	31.8	269.7	112.6	1.0
					42.1	221.3	113.0	4.3
							122.8	0.6
					47.8	231.5	113.7	12.4
					60.4	246.2	113.6	17.2
							123.4	6.3
AMS-6PB	56.9	379.6	0.4	43.8	13.1	245.1		
	56.9	330.1	0.3	43.6	22.5	255.8		
	56.9	197.7	0.2	40.3	28.4	256.5	112.7	0.04
					41.2	261.1	113.1	1.7
					51.9	228.1	113.1	7.6
							122.9	0.07
					60.3	243.7	113.7	15.1
							123.2	0.7
SBA-15PB	109.7	271.9	0.5	97.5	12.1	229.8		
	109.7	245.9	0.4	90.2	19.1	232.2		
	109.7	145.9	0.3	87.9	29.9	238.9	112.2	0.3
		68.8	0.1	87.8	41.5	237.5	113.1	2.3
		12.5	0.03	87.2	49.5	227.0	113.6	12.3
							122.8	1.8
					56.4	238.8	113.7	18.1
							123.1	3.2

[a] Unit cell from powder XRD.
[b] Specific surface area.
[c] Total pore volume and pore size distribution.
[d] Decomposition temperature for the largest TGA weight loss peak.

likely due to the evaporation of water, as silica has been demonstrated to be highly hydrophilic (Fig. S4 insert) (Cordeiro et al., 2016). With the increase in drug loading, a shift in the water desorption endotherm to a lower temperature suggested the adsorption of crystalline PB increased the hydrophobicity of the sample. Therefore, drug loadings above complete pore filling were likely to cause a reduction in drug release kinetics, due to the increase in the amount of recrystallized, hydrophobic PB in these samples.

In vitro dissolution experiments were conducted under sink conditions in simulated intestine fluid (SIF). They generally follow a bimodal drug release pattern consisting of an initial burst, followed by the slower release of PB (Figs. 3a, S6). The burst release at drug loadings < 30 wt% was due to the release of amorphous PB from the mesopores. Drug loadings above complete pore filling caused the reduction in drug release kinetics (Table ST1), likely due to the presence of recrystallized PB on the silica surface. Full release of PB was achieved below this loading level except for MCM-41, where only MCM-41 PB13.1% releases the full amount of the drug loaded (Fig. S6). This may indicate a strong dependency of release kinetics on the diffusion properties of the dissolution media for the smaller pore material (McCarthy et al., 2017). The optimal loading amount of PB in SBA-15 and AMS-6 is 30 wt%, and 20 wt% for MCM-41 (Fig. 3b).

In order to better understand the dissolution kinetics of PB, dose dependent release profiles were measured between 30 and 100 mg. These are shown in the ESI Figs. S7 and S8. Only a small increase in the total amount of PB released is observed at higher doses. This is accompanied by a reduction in the overall percentage of drug released and a loss of sink conditions. Thus, at a dose of 100 mg the formulation of SBA-15PB29.9%, only releases 67% of the loaded PB after 24 h. This trend is observed for all mesoporous materials in this work irrespective of pore size and indicates that PB reaches its saturation state > 30 wt% within the dissolution media (Kjellman et al., 2014).

The mechanism of free radical termination by PB is based on the reaction of its two phenolic hydrogens with ROS to form spiroquinone or diphenoquinone (Barnhart et al., 1989). However, the antioxidant response of PB is limited by its low solubility (Colle et al., 2013). In an *in vivo* study (Betge et al., 2007), oral administration of PB in rats was not effective in scavenging ROS mediated cardiac remodeling after myocardial infarction, as therapeutic concentrations of the drug was not achieved. In comparison to PB, ascorbic acid is a water soluble antioxidant. Upon interaction with a ROS, ascorbic acid acts as an electron donor to quench unstable free radicals, protecting biological molecules from oxidative damage (Padayatty et al., 2003). Ascorbic acid was chosen as an example of a highly potent water soluble compound to compare its antioxidant properties to that of the poorly soluble drug PB.

The antioxidant properties of the test compounds at 100 μM concentration were initially tested in the hCMEC/D3 cell line. In this cell model, the ROS H_2O_2 and the test compound were incubated together with the endothelial cells, and the extracellular scavenging efficacy of the antioxidants was determined by analyzing the percentage of cells under oxidative stress (%ROS +) compared to cells that were not (% ROS -) using the Muse® oxidative stress kit. Fig. 4a shows the % ROS + cells after 24 h incubation with H_2O_2 at different concentrations with or without PB, AMS-6 PB28.4% or ascorbic acid. %ROS - cells are shown in Fig. S9a. In comparison to the positive control, PB released from AMS-6 resulted in higher scavenging response evidenced by a decrease in %ROS + cells when incubated together with H_2O_2 at concentrations below 1000 μM. At the higher concentration of 1500 μM only limited improvement in antioxidant effect was observed. In a subsequent time dependent study, hCMEC/D3 cells were incubated with the test compound and 1000 μM H_2O_2. AMS-6PB28.4% consistently resulted in a decreased number of %ROS + cells (Fig. 4b), in comparison to ascorbic acid or PB alone.

Hydrogen peroxide is a potent ROS that causes degradation to DNA, peroxidation of lipid membranes, and cell death (Shaji et al., 2019). At concentrations > 100 μM, H_2O_2 is known to cause a significant increase in endothelial cell permeability, disruption to cellular membrane protein expression, and decrease in cell viability (Shaji et al., 2019). This is consistent with results from this study as the incubation of endothelial cells with 1000 μM H_2O_2 from 2 to 24 h (positive control) caused the increase in %ROS + cells, and reduction in %viable cells (Fig. S10). The increase in cell death was likely associated with the oxidation of cellular membranes by H_2O_2. Treatment with AMS-6 PB28.4% was shown to delay the increase in %ROS + and cell death, suggesting the release of the amorphous PB from mesoporous silica was more efficient in free radical scavenging, and protecting the hCMEC/D3 cells from oxidative damage by H_2O_2.

In the second cellular model, microglia cells were used to further investigate the antioxidant properties of ascorbic acid, PB, and AMS-6PB28.4%. In the activated state, microglia releases proinflammatory cytokines, and ROS that are part of the immune response to neurotoxins (Thameem Dheen et al., 2007). Oxidative damage by the chronic release of ROS superoxide and nitric oxide cause neuronal cell death, and the development of brain diseases such as depression, Alzheimer's and Parkinson's (Popa-Wagner et al., 2013; Cobourne-Duval et al., 2016). Microglia cells were activated by incubation with 10 μg/ml LPS for 48 h to induce intracellular production of ROS, and were subsequently treated with the test compounds at 1 μM concentration. In the positive control, incubation with LPS without test compounds resulted in the significant increase in %ROS + cells to 75% after 24 h (Fig. 5a). Furthermore, a significant increase in cell death was observed from the

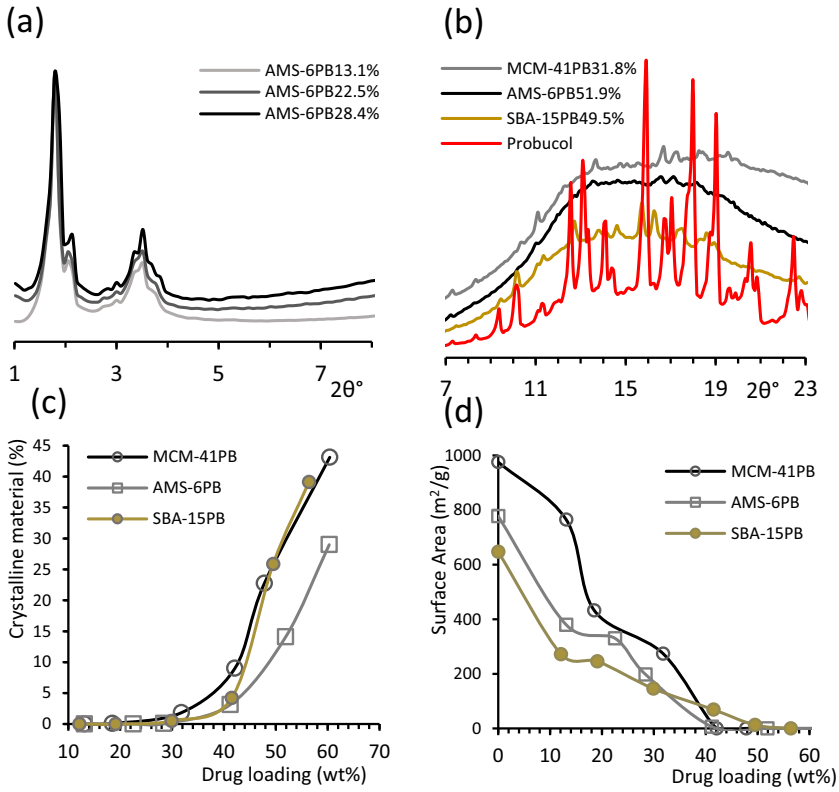

Fig. 2. (a) Diffractograms for drug loaded mesoporous AMS-6 normalized to the most intense peaks. See ESI (Fig. S3) for other materials. No changes to mesoscale order are observed. (b) X-ray diffractograms of drug loaded mesoporous samples at high loading showing the presence of crystalline PB on the external particle surface. These are absent at lower loadings. (c) Percentage amount of crystalline material estimated from differential scanning calorimetry. (d) Decrease in surface area as a function of loading amount as measured by nitrogen adsorption isotherms.

positive control compared to the other samples (Fig. S11a). Treatment with AMS-6PB28.4%, and ascorbic acid resulted in a significant reduction in %ROS + cells compared to PB, and positive control after 6 h (Fig. 5a). No statistical significance was observed between treatment with ascorbic acid or AMS-6 PB28.4% in terms of %ROS + or cell viability. A significant enhancement in antioxidant response was observed in AMS-6PB28.4% compared to PB after 6 h incubation.

The antioxidant response of PB was limited by its low solubility in aqueous media, a result consistent with previous findings (Horwitz et al., 1996; Betge et al., 2007). The release of PB from its amorphous state with superior solubility, and release kinetics led to the enhancement in H_2O_2 scavenging efficiency, protecting hCMEC/D3 cells against oxidative stress, and cell death in an extracellular ROS model. Treatment with either PB or ascorbic acid did not result in an overall reversal of %ROS + hCMEC/D3 cells, likely due to the high concentration of H_2O_2 used in this study. In the second cell model, activation of microglia cells by LPS was used to determine the efficacy of the test compounds in scavenging intracellular ROS levels. The antioxidant

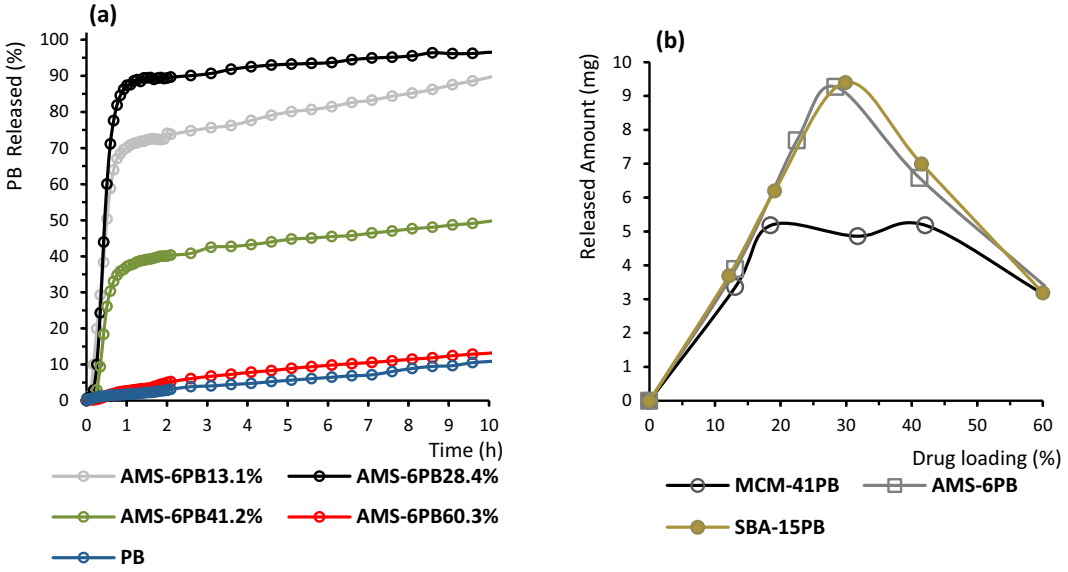

Fig. 3. Results from *in vitro* dissolution studies (a) Kinetic release profile of AMS-6 PB at different loading amounts, showing the initial burst release is followed by a slower rate of drug release. A reduction in % release of PB was observed at high drug loadings. See ESI (Fig. S6) for other materials. (b) Total amount of PB released from a 30 mg capsule dose of drug loaded mesoporous silica particles. Complete drug release was achieved up to 30 wt% drug loading in AMS-6 and SBA-15 mesoporous silica particles.

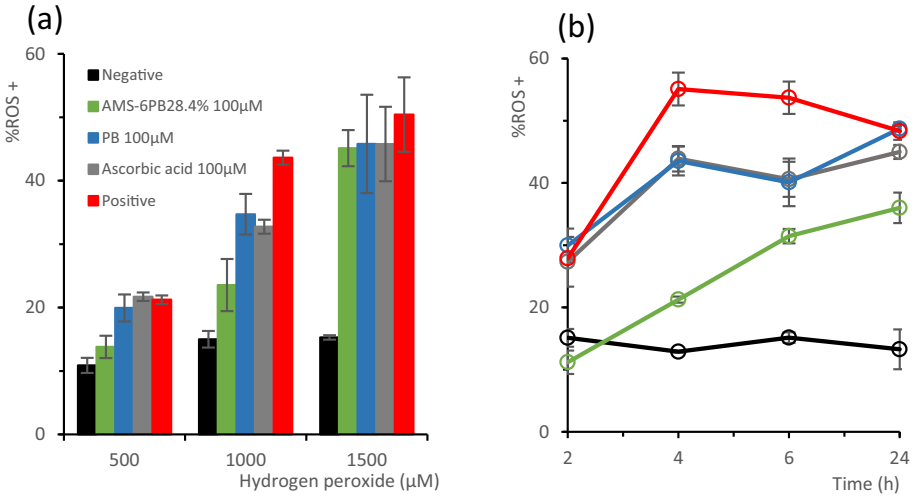

Fig. 4. (a) %ROS + cells (hCMEC/D3) after 24 h incubation with different concentrations of hydrogen peroxide (500 μM to 1500 μM) together with the test compounds. The positive control is hydrogen peroxide alone whilst the negative control represents normal cell growth with no hydrogen peroxide. (b) Evolution of antioxidant activity of test samples between 2 and 24 h incubation with 1000 μM hydrogen peroxide plotted as a function of %ROS + cells (hCMEC/D3). See Fig. S9 for %ROS - data.

response is shown to be dependent on the dissolution rate of PB in aqueous media, with a faster effect observed for PB released from mesoporous silica. The scavenging of intracellular ROS is likely to be enhanced by silica particle uptake across the cell membrane of the macrophages, which has been found to be rapid and favorable for mesoporous AMS-6 particles (Witasp et al., 2009). Therefore, results from the *in vitro* work in the two cellular models indicate the release of amorphous PB from mesoporous AMS-6 can enhance the antioxidant response to extracellular or intracellular ROS. This can potentially open new therapeutic applications for mesoporous silica loaded PB in the treatment of diseases associated with oxidative stress, where rapid quenching of free radicals are required such as in treatment of cardiovascular diseases (Moris et al., 2017).

4. Conclusion

The enhancement of dissolution of extremely lipophilic pharmaceutical compounds is demonstrated using PB as a model drug. Whilst the dissolution improvement is significant, the maximum loading capacity of PB within the pores of mesoporous materials is optimal at 30 wt%, above which the compound crystallizes primarily as the form II polymorph on the external surface. Release kinetics is fastest in the absence of crystalline material and at doses below 40 mg. In comparison to the excipient polyvinylpyrrolidone K-30 (Thybo et al., 2008) or co-milling techniques (Li et al., 2017), a faster release kinetics is observed here with > 80% of the loaded amount released within the first hour for SBA-15 and AMS-6 mesoporous silica formulations. At high loadings above 30 wt% and 40 mg doses the solubilized compound quickly reaches saturation. The released PB has improved antioxidant behavior in comparison to the crystalline form, which may enable its use in new therapeutic areas where solubility and rapid therapeutic kinetics are required such as for the treatment of cardiovascular diseases.

Declaration of competing interest

AEGB is the co-founder of Nanologica AB (Stockholm, Sweden) a company commercializing nanoporous materials for biomedical applications. No other co-authors report any potential conflict of interest.

Acknowledgements

This work was partly financed through support from the ARC Centre of Excellence for Nanoscale BioPhotonics (CE140100003), an ARC Future Fellowship (AEGB, FT150100342) as well as a Macquarie University Infrastructure grant (MQRIBG 9201501951). AEGB would like to thank Macquarie University's Microscopy Unit for access to SEM facilities.

Appendix A. Supplementary data

Supplementary data to this article can be found online at https://doi.org/10.1016/j.ejps.2019.105038.

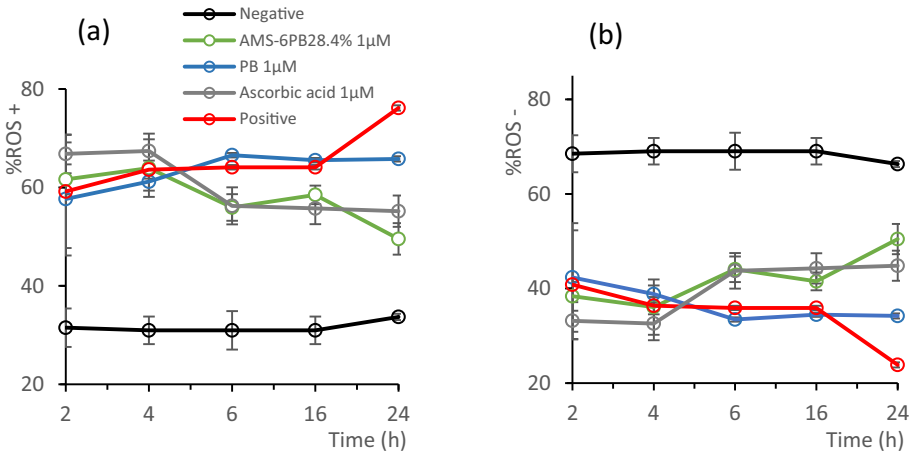

Fig. 5. (a) %ROS + microglia cells and (b) %ROS – microglia cells after incubation with test compounds for 2 to 24 h. Microglia cells were activated by incubation with 10 μg/ml LPS for 48 h, after which cells were incubated with test compounds for 2 to 24 h. Positive was activated microglia cells without incubation with test compounds, and negative was microglia cells without activation with LPS.

References

Atluri, R., Hedin, N., Garcia-Bennett, A.E., 2008. Hydrothermal phase transformation of bicontinuous cubic mesoporous material AMS-6. Chem. Mater. 20, 3857–3866.

Balbi, M.E., Tonin, F.S., Mendes, A.M., Borba, H.H., Wiens, A., Fernandez-Llimos, F., Pontarolo, R., 2018. Antioxidant effects of vitamins in type 2 diabetes: a meta-analysis of randomized controlled trials. Diabetol. Metab. Syndr. 10, 18.

Barnhart, R.L., Busch, S.J., Jackson, R.L., 1989. Concentration-dependent antioxidant activity of probucol in low density lipoproteins in vitro: probucol degradation precedes lipoprotein oxidation. J. Lipid Res. 30, 1703–1710.

Baynes, J.W., 1991. Role of oxidative stress in development of complications in diabetes. Diabetes 40, 405–412.

Betge, S., Lutz, K., Roskos, M., Figulla, H.-R., 2007. Oral treatment with probucol in a pharmacological dose has no beneficial effects on mortality in chronic ischemic heart failure after large myocardial infarction in rats. Eur. J. Pharmacol. 558, 119–127.

Birben, E., Sahiner, U.M., Sackesen, C., Erzurum, S., Kalayci, O., 2012. Oxidative stress and antioxidant defense. World Allergy Organ. J. 5, 9.

Brunauer, S., Emmett, P.H., Teller, E., 1938. Adsorption of gases in multimolecular layers. J. Am. Chem. Soc. 60, 309–319.

Chartoumpekis, D., Ziros, P.G., Psyrogiannis, A., Kyriazopoulou, V., Papavassiliou, A.G., Habeos, I.G., 2010. Simvastatin lowers reactive oxygen species level by Nrf2 activation via PI3K/Akt pathway. Biochem. Biophys. Res. Commun. 396, 463–466.

Cobourne-Duval, M.K., Taka, E., Mendonca, P., Bauer, D., Soliman, K.F., 2016. The antioxidant effects of thymoquinone in activated BV-2 murine microglial cells. Neurochem. Res. 41, 3227–3238.

Colle, D., Santos, D.B., Moreira, E.L.G., Hartwig, J.M., dos Santos, A.A., Zimmermann, L.T., Hort, M.A., Farina, M., 2013. Probucol increases striatal glutathione peroxidase activity and protects against 3-nitropropionic acid-induced pro-oxidative damage in rats. PLoS One 8, e67658.

Cordeiro, T., Santos, A.F., Nunes, G., Cunha, G., Sotomayor, J., Fonseca, I.M., Danède, F., Dias, C., Cardoso, M.M., Correia, N., 2016. Accessing the physical state and molecular mobility of naproxen confined to nanoporous silica matrixes. J. Phys. Chem. C 120, 14390–14401.

Day, B.J., 2004. Catalytic antioxidants: a radical approach to new therapeutics. Drug Discov. Today 9, 557–566.

de Cavanagh, E.M., Inserra, F., Toblli, J., Stella, I., Fraga, C.G., Ferder, L., 2001. Enalapril attenuates oxidative stress in diabetic rats. Hypertension 38, 1130–1136.

Di Meo, S., Reed, T.T., Venditti, P., Victor, V.M., 2016. Role of ROS and RNS sources in physiological and pathological conditions. Oxidative Med. Cell. Longev. 2016.

Gerber, J.J., Caira, M.R., Lötter, A.P., 1993. Structures of two conformational polymorphs of the cholesterol-lowering drug probucol. J. Crystallogr. Spectrosc. Res. 23, 863–869.

Grün, M., Unger, K.K., Matsumoto, A., Tsutsumi, K., 1999. Novel pathways for the preparation of mesoporous MCM-41 materials: control of porosity and morphology. Microporous Mesoporous Mater. 27, 207–216.

Holvoet, P., 2008. Relations between metabolic syndrome, oxidative stress and inflammation and cardiovascular disease. Verh. K. Acad. Geneeskd. Belg. 70, 193–219.

Horwitz, L.D., Wallner, J.S., Decker, D.E., Buxser, S.E., 1996. Efficacy of lipid soluble, membrane-protective agents against hydrogen peroxide cytotoxicity in cardiac myocytes. Free Radic. Biol. Med. 21, 743–753.

Hu, Y., Zhi, Z., Zhao, Q., Wu, C., Zhao, P., Jiang, H., Jiang, T., Wang, S., 2012. 3D cubic mesoporous silica microsphere as a carrier for poorly soluble drug carvedilol. Microporous Mesoporous Mater. 147, 94–101.

Jangra, S., Girotra, P., Chhokar, V., Tomer, V., Sharma, A., Duhan, S., 2016. In-vitro drug release kinetics studies of mesoporous SBA-15-azathioprine composite.

Kizhakekuttu, T.J., Widlansky, M.E., 2010. Natural antioxidants and hypertension: promise and challenges. Cardiovasc. Ther. 28, e20–e32.

Kjellman, T., Xia, X., Alfredsson, V., Garcia-Bennett, A.E., 2014. Influence of microporosity in SBA-15 on the release properties of anticancer drug dasatinib. J. Mater. Chem. B 2, 5265–5271.

Kruk, M., Jaroniec, M., Ko, C.H., Ryoo, R., 2000. Characterization of the porous structure of SBA-15. Chem. Mater. 12, 1961–1968.

Kukin, M.L., Kalman, J., Charney, R.H., Levy, D.K., Buchholz-Varley, C., Ocampo, O.N., Eng, C., 1999. Prospective, randomized comparison of effect of long-term treatment with metoprolol or carvedilol on symptoms, exercise, ejection fraction, and oxidative stress in heart failure. Circulation 99, 2645–2651.

Kuzuya, M., Kuzuya, F., 1993. Probucol as an antioxidant and antiatherogenic drug. Free Radic. Biol. Med. 14, 67–77.

Li, J., Yang, Y., Zhao, M., Xu, H., Ma, J., Wang, S., 2017. Improved oral bioavailability of probucol by dry media-milling. Mater. Sci. Eng. C 78, 780–786.

Mahajan, A.S., Babbar, R., Kansal, N., Agarwal, S.K., Ray, P.C., 2007. Antihypertensive and antioxidant action of amlodipine and vitamin C in patients of essential hypertension. J. Clin. Biochem. Nutr. 40, 141–147.

Maleki, A., Hamidi, M., 2016. Dissolution enhancement of a model poorly water-soluble drug, atorvastatin, with ordered mesoporous silica: comparison of MSF with SBA-15 as drug carriers. Expert Opin. Drug Deliv. 13, 171–181.

Maleki, A., Kettiger, H., Schoubben, A., Rosenholm, J.M., Ambrogi, V., Hamidi, M., 2017. Mesoporous silica materials: from physico-chemical properties to enhanced dissolution of poorly water-soluble drugs. J. Control. Release 262, 329–347.

Manzano, M., Aina, V., Arean, C., Balas, F., Cauda, V., Colilla, M., Delgado, M., Vallet-Regi, M., 2008. Studies on MCM-41 mesoporous silica for drug delivery: effect of particle morphology and amine functionalization. Chem. Eng. J. 137, 30–37.

McCarthy, C.A., Ahern, R.J., Devine, K.J., Crean, A.M., 2017. Role of drug adsorption onto the silica surface in drug release from mesoporous silica systems. Mol. Pharm. 15, 141–149.

Moris, D., Spartalis, M., Spartalis, E., Karachaliou, G.-S., Karaolanis, G.I., Tsourouflis, G., Tsilimigras, D.I., Tzatzaki, E., Theocharis, S., 2017. The role of reactive oxygen species in the pathophysiology of cardiovascular diseases and the clinical significance of myocardial redox. Ann. Transl. Med. 5.

Nielsen, F.S., Petersen, K.B., Müllertz, A., 2008. Bioavailability of probucol from lipid and surfactant based formulations in minipigs: influence of droplet size and dietary state. Eur. J. Pharm. Biopharm. 69, 553–562.

O'Brien, R.C., Luo, M., Balazs, N., Mercuri, J., 2000. In vitro and in vivo antioxidant properties of gliclazide. J. Diabetes Complicat. 14, 201–206.

Padayatty, S.J., Katz, A., Wang, Y., Eck, P., Kwon, O., Lee, J.-H., Chen, S., Corpe, C., Dutta, A., Dutta, S.K., 2003. Vitamin C as an antioxidant: evaluation of its role in disease prevention. J. Am. Coll. Nutr. 22, 18–35.

Popa-Wagner, A., Mitran, S., Sivanesan, S., Chang, E., Buga, A.-M., 2013. ROS and brain diseases: the good, the bad, and the ugly. Oxidative Med. Cell. Longev. 2013.

Pourova, J., Kottova, M., Voprsalova, M., Pour, M., 2010. Reactive oxygen and nitrogen species in normal physiological processes. Acta Physiol. 198, 15–35.

Prasad, B.R., Lele, S., 1994. Stabilization of the amorphous phase inside carbon nanotubes: solidification in a constrained geometry. Philos. Mag. Lett. 70, 357–361.

Ravikovitch, P.I., Vishnyakov, A., Neimark, A.V., Ribeiro Carrott, M.M.L., Russo, P.A., Carrott, P.J., 2006. Characterization of micro-mesoporous materials from nitrogen and toluene adsorption:experiment and modeling. Langmuir 22, 513–516.

Redón, J., Oliva, M.R., Tormos, C., Giner, V., Chaves, J., Iradi, A., Sáez, G.T., 2003. Antioxidant activities and oxidative stress byproducts in human hypertension. Hypertension 41, 1096–1101.

Rengarajan, G., Enke, D., Steinhart, M., Beiner, M., 2008. Stabilization of the amorphous state of pharmaceuticals in nanopores. J. Mater. Chem. 18, 2537–2539.

Rodrigo, R., Prat, H., Passalacqua, W., Araya, J., Guichard, C., Bächler, J.P., 2007. Relationship between oxidative stress and essential hypertension. Hypertens. Res. 30, 1159.

Shaji, C.A., Robinson, B.D., Yeager, A., Beeram, M.R., Davis, M.L., Isbell, C.L., Huang, J.H., Tharakan, B., 2019. The tri-phasic role of hydrogen peroxide in blood-brain barrier endothelial cells. Sci. Rep. 9, 133.

Singh, R., Gupta, B., Tripathi, K., Singh, S., 2016. Anti oxidant potential of metformin and pioglitazone in type 2 diabetes mellitus: beyond their anti glycemic effect. Diabetes Metab. Syndr. Clin. Res. Rev. 10, 102–104.

Tanaka, Y., Inkyo, M., Yumoto, R., Nagai, J., Takano, M., Nagata, S., 2012. Nanoparticulation of probucol, a poorly water-soluble drug, using a novel wet-milling process to improve in vitro dissolution and in vivo oral absorption. Drug Dev. Ind. Pharm. 38, 1015–1023.

Thameem Dheen, S., Kaur, C., Ling, E.-A., 2007. Microglial activation and its implications in the brain diseases. Curr. Med. Chem. 14, 1189–1197.

Thybo, P., Pedersen, B.L., Hovgaard, L., Holm, R., Müllertz, A., 2008. Characterization and physical stability of spray dried solid dispersions of probucol and PVP-K30. Pharm. Dev. Technol. 13, 375–386.

Wassmann, S., Laufs, U., Müller, K., Konkol, C., Ahlbory, K., Bäumer, A.T., Linz, W., Böhm, M., Nickenig, G., 2002. Cellular antioxidant effects of atorvastatin in vitro and in vivo. Arterioscler. Thromb. Vasc. Biol. 22, 300–305.

Witasp, E., Kupferschmidt, N., Bengtsson, L., Hultenby, K., Smedman, C., Paulie, S., Garcia-Bennett, A.E., Fadeel, B., 2009. Efficient internalization of mesoporous silica particles of different sizes by primary human macrophages without impairment of macrophage clearance of apoptotic or antibody-opsonized target cells. Toxicol. Appl. Pharmacol. 239, 306–319.

Wu, S.-H., Mou, C.-Y., Lin, H.-P., 2013. Synthesis of mesoporous silica nanoparticles. Chem. Soc. Rev. 42, 3862–3875.

Xu, W., Riikonen, J., Lehto, V.-P., 2013. Mesoporous systems for poorly soluble drugs. Int. J. Pharm. 453, 181–197.

Yamashita, S., Masuda, D., Matsuzawa, Y., 2015. Did we abandon probucol too soon? Curr. Opin. Lipidol. 26, 304–316.

Zhang, Z., Jiang, S., Liu, Z., Niu, B., Gu, W., Li, Y., Cui, J., 2014. Directed self-assembled nanoparticles of probucol improve oral delivery: fabrication, performance and correlation. Pharm. Res. 31, 2266–2275.